Sager, W.W., Kanazawa, T., and Escutia, C. (Eds.)
Proceedings of the Ocean Drilling Program, Scientific Results Volume 191

4. Geochemical Study of ODP Leg 191 Site 1179 Sediments: Direct Observation of Mn and Ce Oxidation States[1]

M. Fukukawa,[2] Y. Takahashi,[2] Y. Hayasaka,[2] Y. Sakai,[3] and H. Shimizu[2]

ABSTRACT

Depth profiles of major element and rare earth element (REE) abundances in sediment samples (mainly siliceous ooze and clay) recovered from Holes 1179B and 1179C at Site 1179, Ocean Drilling Program Leg 191 (41.4°N, 159.6°E) were determined. The oxidation states of Mn and Ce were determined by X-ray absorption near-edge structure. Some geochemical indicators were tested, including the MnO/TiO_2 ratios, a bivariate diagram of La/Ce vs. $Al_2O_3/(Al_2O_3+Fe_2O_3)$, and other discrimination diagrams. The oxidation state of Mn is reduced Mn(II) in the depth profile below 0.60 meters below seafloor (mbsf), which is consistent with relatively low and high abundances of Mn in the sediments and pore waters, respectively. It is possible that the diagenetic effect on the oxidation state and abundance of Mn makes it difficult for the MnO/TiO_2 ratio to reflect the depositional environment. The normalized ratio of La and Ce does not change very much with depth, suggesting that the diagenetic effect does not affect the REE signature in the sediments. On the diagram of La/Ce vs. $Al_2O_3/(Al_2O_3+Fe_2O_3)$, the sediments studied here plot at the boundary of the pelagic and continental margin fields. This suggests that continental material has contributed to the sediment to some degree, even though Site 1179 is in a pelagic region of the northwestern Pacific Ocean, >1600 km from Japan.

[1]Fukukawa, M., Takahashi, Y., Hayasaka, Y., Sakai, Y., and Shimizu, H., 2004. Geochemical study of ODP Leg 191 Site 1179 sediments: direct observation of Mn and Ce oxidation states. *In* Sager, W.W., Kanazawa, T., and Escutia, C. (Eds.), *Proc. ODP, Sci. Results,* 191, 1–24 [Online]. Available from World Wide Web: <http://www-odp.tamu.edu/publications/191_SR/VOLUME/CHAPTERS/007.PDF>. [Cited YYYY-MM-DD]
[2]Department of Earth and Planetary Systems Science, Graduate School of Science, Hiroshima University, Higashi-Hiroshima, Hiroshima 739-8526, Japan. Correspondence author: takahasi@geol.sci.hiroshima-u.ac.jp
[3]Department of Chemistry, Daido Institute of Technology, Takiharu-cho, Minami-ku, Nagoya 457-8530, Japan.

Initial receipt: 17 January 2003
Acceptance: 18 April 2004
Web publication: 6 August 2004
Ms 191SR-007

INTRODUCTION

The abundances of trace elements in sedimentary rocks have been employed to elucidate the sources and formation environment of the sediments. For example, it is suggested that a cerium anomaly found in the rare earth element (REE) patterns of chert reflects its depositional environment, that is, whether it was deposited in the marginal sea, the continental shelf, or the deep-ocean floor (Shimizu and Masuda, 1977). Murray (1994) developed a similar method in chert and employed a diagram on which he plotted the ratio of La and Ce against the ratio $Al_2O_3/(Al_2O_3+Fe_2O_3)$. The MnO/TiO_2 ratio can be another indicator of the depositional environment (Sugisaki et al., 1982; Yamamoto, 1983; Sugisaki, 1984; Sugitani, 1996). To use these abundance data (Al, Ti, Mn, Fe, La, and Ce) as geochemical signatures, it is necessary to carefully study various factors, such as diageneis, that can alter the initial signature. In particular, redox-sensitive elements can be mobilized during early diagenesis, altering the initial geochemical signatures. However, there have been few studies on the direct characterization of the oxidation states of elements in sediments using proper physico-chemical methods (except for iron, which has been studied by Mössbauer spectroscopy).

Sediments recovered from ODP Leg 191 Site 1179 (41.4°N, 159.6°E; water depth = 5565 m) located on the abyssal seafloor northwest of Shatsky Rise, ~1600 km east of Japan (Fig. F1), are mainly siliceous ooze and clay overlaying cherty rocks (Kanazawa, Sager, Escutia, et al., 2001). We studied the oxidation states of Mn and Ce by X-ray absorption near-edge structure (XANES) on samples throughout the sediment core. It is considered that these elements are immobile in their oxidized forms (Mn[IV] and Ce[IV]), whereas they may be more mobile in their reduced forms (Mn[II] and Ce[III]). Therefore, we compared the depth profiles of abundances and oxidation states of these elements in the sediment core at Site 1179. The direct determination of the oxidation states of these elements was used to explain the variation of abundances of Mn and Ce in the sediments. Other discrimination diagrams based on major element abundances are employed to compare the information obtained from the MnO/TiO_2 ratio and REE signature.

F1. Site 1179 map, p. 11.

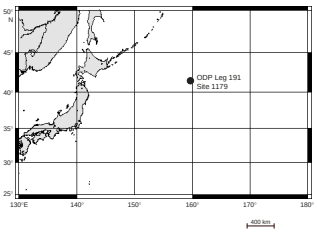

SAMPLES

Four sedimentary units, with a total thickness of 377 m, overlie basaltic crust at Site 1179 (Kanazawa, Sager, Escutia, et al., 2001). Unit I, at the top of the section, consists of clay- and radiolarian-bearing diatom ooze. It extends from the seafloor to a depth of 223.5 meters below seafloor (mbsf), where it is late Miocene in age. Sediments from 0.01 to 35.0 mbsf were used in this study. The uppermost sediment samples from 0.01 to 1.81 mbsf were recovered from Core 191-1179C-1H. Samples at greater depths were recovered from Cores 191-1179B-1H through 4H, which cover depths between 0.60 and 35.00 mbsf. The precise depth of each sample examined in this study is shown in Table T1, along with the major element composition.

T1. Major element composition of sediment samples, p. 23.

The core recovered at Site 1179 is of a typical abyssal sediment overlying chert (Kanazawa, Sager, Escutia, et al., 2001). Brief sample descriptions are given in Table T1. Diatoms predominate over the collected depth range, and radiolarians are common. Sponge spicules and silico-

flagellates also contribute to the siliceous nature of the sediment. The sediment can be regarded as a precursor of chert or siliceous shale. In addition to the biogenic silica component, the sediment includes clay and ash.

ANALYTICAL METHODS

Sediments were recovered from Cores 191-1179B-1H through 4H under N_2 atmosphere to minimize exposure to oxygen. A part of each sample was packed in an airtight bag. These samples were used for XANES analysis to determine the oxidation states of Mn and Ce. The remainder of each sample was washed twice with Milli-Q water and dried for chemical analysis.

The major element composition of the sediment samples were determined by X-ray fluorescence (XRF) spectroscopy (Rigaku ZSX-101e). The samples were dried overnight at 110°C. The fusion glass was made from a mixture of sample (2.00 g), flux (4.00 g; $Li_2B_4O_7$:$LiBO_2$ = 1:4, Johnson Matthey Spectro flux 100B), and $LiNO_3$ (0.60 g). Details of the procedure used for the XRF analysis are found in Kanazawa, Sager, Escutia, et al. (2001). Abundances of the REE were measured using an inductively coupled plasma–mass spectrometer (ICP-MS) as described previously (Takahashi et al., 2002b). Approximately 0.1 g of sediment sample was first digested in a mixture of $HClO_4$ and HF, and the solution was then redissolved into $HClO_4$ after being dried. The sample was redissolved in HCl and evaporated. The residue was redissolved using 2% HNO_3 for measurement with ICP-MS using In and Bi as internal standards.

XANES spectra were recorded at BL-12C in the Photon Factory, KEK (Tsukuba, Japan) (Nomura and Koyama, 1996), or at BL01B1 in SPring-8 (Hyogo, Japan) (Uruga et al., 1999). Experimental procedures are similar to those in Takahashi et al. (2002a). A Si(111) double-crystal monochromator was used to obtain the incident X-ray beam. The energy step was typically 0.25 eV. The energy of the peak top did not shift >0.25 eV throughout all measurements. All spectra were collected in the fluorescence mode with the sample positioned at an angle of 45° with respect to the beam. The fluorescence yield was measured using a 19-element Ge semiconductor detector. It was necessary to correct the single-channel analyzer windowed signal because of the increase in dead time when the incoming count rate was high because of the large intensity from fluorescence and scattered X-rays.

RESULTS AND DISCUSSION

Abundance and Oxidation State of Mn

In the depth region studied here, the sedimentation rate is ~30 m/m.y. (from paleomagnetic data: Kanazawa, Sager, Escutia, et al., 2001) and the content of organic carbon ranges from 0.10 to 0.50 wt% (Table **T1**). Stein (1986, 1990) classified the sediments on the basis of the sedimentation rate and the content of organic carbon. According to this classification, the samples studied here are formed under an open-ocean environment. This is also indicated by the concentration profiles of dissolved sulfate in pore water against depth (Kanazawa, Sager, Escutia, et al., 2001). The dissolved sulfate concentration is >24 mM, which indicates that sulfate reduction is not the predominant mechanism for

the decomposition of organics in this region (Fig. F2). Dissolved nitrate is observed even at 5 mbsf, and ammonium increases steadily with depth (Kanazawa, Sager, Escutia, et al., 2001). The maximum of dissolved Mn is found at ~6 mbsf (Fig. F2) (Kanazawa, Sager, Escutia, et al., 2001). These results suggest that the sediment at Site 1179 is in a fairly oxic condition.

The major element composition of the sediment samples is shown in Table T1. The silica content of the sediment samples ranges from 56 to 66 wt%, and the Al_2O_3 content is between 11 and 17 wt%, mainly because of the presence of clay minerals. As expected, the MnO content is highest near the seafloor (0.31 mbsf). This is due to the upward diffusion flux of dissolved manganese within the sediments. Evidence for this is the increase in dissolved manganese with depth up to 6 mbsf (Fig. F2). Near the sediment/water interface, reduced manganese (Mn^{2+}) is oxidized to Mn(IV), as shown by the direct observation of the oxidation state of Mn.

The oxidation state of manganese (Mn^{4+}/Mn^{2+} ratio) can be elucidated by the shift of the pre-edge peak in the Mn K-edge XANES spectrum (Schulze et al., 1995). Qualitatively, it is observed that the whole spectrum shifts to higher energy because of the increase in the attractive force between the electrons and the nucleus when the effective positive charge of the nucleus increases (i.e., at a higher oxidation state). To determine the average valence of Mn, XANES spectra of reference materials made by mixing δ-MnO_2 and $MnSO_4$ were measured (Fig. F3A). The pre-edge structure was fitted by the combination of a Gaussian function and a second-order polynomial function (Schulze et al., 1995). The calibration line between the average valence of Mn and the shift of the peak defined by the centroid of the Gaussian function is shown in Figure F3B, suggesting that the average valence of Mn can be estimated by the pre-edge structure. The XANES spectra at the pre-edge region for the sediment samples are shown in Figure F3C. It is clear that Mn is more oxidized at 0.60 mbsf compared with Mn at 1.82 mbsf. The depth profile of the average valence of Mn (Fig. F4) shows that Mn in the sediment is mainly divalent below 0.60 mbsf. The reduced state of Mn at depth, as determined directly by XANES, is consistent with the results of the depth profiles of Mn abundances in sediments and pore water.

Sugisaki and his coworkers (Sugisaki et al., 1982; Yamamoto, 1983; Sugisaki, 1984; Sugitani, 1996) suggested that the MnO/TiO_2 ratio can be used to distinguish pelagic and continental sources of siliceous sediments. Sugitani (1996) studied the MnO/TiO_2 ratios of marine sediments at various distances from land. Sugitani (1996) divided these values, plotted in Figure F5, into two groups: sediments <110 km away from land are hemipelagic, and those >600 km are pelagic. We tentatively define the boundary of these two groups at 400 km, which corresponds to an MnO/TiO_2 ratio of ~0.5. This value can be used for classifying sediments into the hemipelagic and pelagic origins. The MnO/TiO_2 ratio of the samples studied here varies from 0.171 to 10.9 (Fig. F6). If we use the value obtained from the sediment samples of Site 1179, the sediments near the seafloor (above 0.6 mbsf) would be classified as pelagic. However, when we use the sediment below ~1 mbsf, the MnO/TiO_2 ratio is more representative of the hemipelagic region. This is caused by the change in Mn concentration, which is a result of the early diagenesis. We suggest that the high mobility of Mn in the sediment column, confirmed by the depth profiles of Mn abundances in the sediments and pore water and the oxidation state of Mn in the sedi-

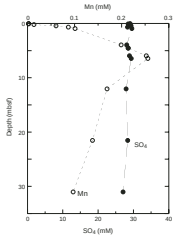

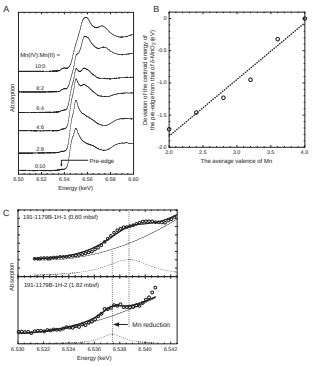

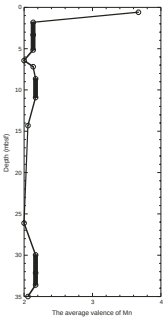

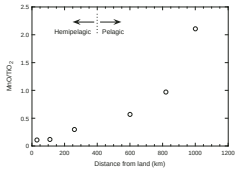

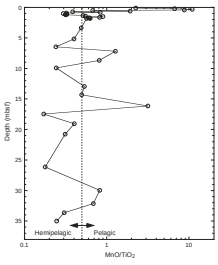

ments by XANES, can obscure the clear characterization of the depositional environment using the MnO/TiO_2 ratio. It is necessary to consider such a diagenetic effect when employing the MnO/TiO_2 ratio to characterize sediments and sedimentary rocks, as has been shown by Murray (1994) and the multiple references therein.

REE Signature and the Oxidation State of Ce

The degree of the Ce anomaly obtained from REE abundances can be employed as another signature of the depositional environment of siliceous sediment. To compare the MnO/TiO_2 ratio and the degree of the Ce anomaly, we also measured the REE abundances in the sediment samples at Site 1179. The results are shown in Table T2. Some of the REE patterns normalized with post-Archean shales from Australia (PAAS) (Taylor and McLennan, 1988) are shown in Figure F7. PAAS was used for the normalization, because the REE pattern of PAAS normalized with the C1 chondrite (Anders and Grevesse, 1989) creates a smooth REE pattern. Although North American Shale Composite (NASC) (Gromet et al., 1984) is generally used to obtain the ratio of normalized abundances of La and Ce, it was not used here for the normalization of the REE patterns of the sediments. This is because the REE pattern of NASC normalized with C1 chondrite did not create a smooth REE pattern, which suggests that the normalization with NASC is not appropriate for the interpretation of the fine structures of REE patterns. It must be noted that the REE patterns of the sediments studied here are similar, which suggests that the chemical processes in this sedimentary setting were rather similar during the past ~1 m.y. (corresponding to a sediment depth of ~35 mbsf). Slight variations in the REE abundances are observed, although the shapes of the REE patterns are very similar. Among the major elements, TiO_2 shows a slight correlation with REE abundances, represented by the Nd content, as shown in Figure F8, where the data from the Hole 1179B cores are plotted. Since the origin of TiO_2 is considered terrigenous, the abundances of REE indicate the influence of terrigenous material within the sediments. The most striking feature recorded in the REE patterns of sediments is the degree of the Ce anomaly, noted as Ce/Ce* (Shimizu and Masuda, 1977):

$$Ce/Ce^* = Ce_N/(La_N\ Pr_N)^{1/2},$$

where N indicates the normalized abundance with a proper reference material. According to Shimizu and Masuda (1977), the normalization was conducted with chondrite. A negative Ce anomaly implies that the sediment was formed under a pelagic environment, whereas a positive or no Ce anomaly implies formation at the continental margin. Murray (1994) summarized the abundances of REE and other elements and provided a discrimination diagram by a bivariate plot of La_N/Ce_N and $Al_2O_3/(Al_2O_3+Fe_2O_3)$. La_N/Ce_N normalized with NASC was used here instead of Ce/Ce*, where the meaning of the La_N/Ce_N ratio is similar to Ce/Ce*. The continental margin sediments contain relatively high amounts of Ce, leading to a low La_N/Ce_N ratio, and the pelagic sediments, depleted in Ce, show a high La_N/Ce_N ratio. The present data, when plotted on this discrimination diagram (Fig. F9), are concentrated near the boundary of the two fields of the pelagic and the continental margin. This indicates that the sediments at Site 1179 exhibit intermediate characteristics between pelagic and continental margin origin.

T2. Abundances of REE in sediment samples, p. 24.

F7. PAAS-normalized REE patterns, p. 17.

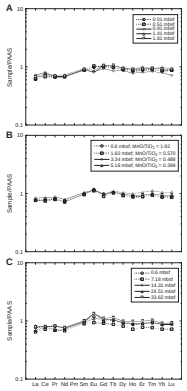

F8. Nd vs. TiO_2, p. 18.

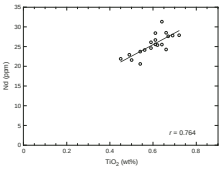

F9. La_N/Ce_N ratio vs. $Al_2O_3/(Al_2O_3 + Fe_2O_3)$, p. 19.

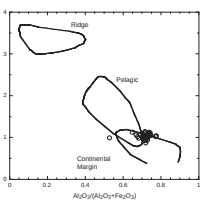

It is possible that the Ce oxidation state can change during diagenetic processes, which may lead to the fractionation of Ce from other REEs and to the alteration of the initial REE signature. We measured Ce L_{III}-edge XANES to elucidate the cerium oxidation state. The selected spectra, with the results of peak deconvolution by the combination of one arctangent and three Lorentzian functions, are shown in Figure **F10.** The peak at ~5.726 keV can be ascribed to Ce(III), and the peaks at 5.730 and 5.738 keV are assigned to Ce(IV) (Takahashi et al., 2000a, 2002a). The XANES spectra show that Ce(III) is predominant in the sediment samples at Site 1179, although it is not obvious whether Ce(IV) is incorporated in the sediments because of the low quality of the spectra. However, it seems that some Ce(IV) (<10% of total Ce) is incorporated in the sediments at 0.60 mbsf. This indicates that the redox change of Ce did not affect the REE patterns of the sediment samples, due to possible diagenetic effects, unlike the variation of the MnO/TiO_2 ratio (Fig. **F7C**). This supports the idea that the REEs, including both Ce(III) and Ce(IV), are fairly immobile during diagenetic processes and that the REE signature is useful to deduce depositional environment of sediments.

In the depth profile of the La_N/Ce_N ratio, a slight decrease in the La_N/Ce_N values near the surface of the sediments was observed, even though the La_N/Ce_N ratio was rather stable throughout the sediment column (Fig. **F11**). It is possible that the slight variation in La_N/Ce_N values is related to the content of Mn, which increases in the subsurface to give larger MnO/TiO_2 ratios, since the MnO_2 phase can accumulate Ce by oxidative sorption of Ce (Takahashi et al., 2000b, and references therein). The enrichment of Ce induces the decrease in the La_N/Ce_N ratio. However, it must be noted that the increase in the MnO/TiO_2 ratio suggests that the deposition took place in a pelagic region, whereas the decrease in the La_N/Ce_N ratio (or enrichment of Ce), presumably caused by the increase of Mn, indicates that the deposition was at the continental margin. This inconsistency between the La_N/Ce_N and MnO/TiO_2 ratios could result from the misuse of geochemical indicators. The large La_N/Ce_N ratio indicates that the deposition was in a pelagic region because the increase in the La_N/Ce_N ratio with deeper seawater was generally observed (e.g., Piepgras and Jacobsen, 1992). If the REEs in the sediments were mainly associated with a mineral phase like silica, the fractionation of Ce by the sediments would have not occurred, which suggests that the Ce anomaly or the La_N/Ce_N ratio of the sediments was similar to that of seawater. In this case, the large La_N/Ce_N ratio suggests that the deposition of the sediments was in a pelagic region. However, if the REE in the sediments was somehow incorporated in the MnO_2 phase, the La_N/Ce_N ratio, smaller than that of seawater, induced by the enrichment of Ce in the sediments may have led to the continental origin. This discussion implies that the La_N/Ce_N ratio should be employed for siliceous sediments for the interpretation of the depositional environment using the ratio.

F10. Cerium L_{III}-edge XANES spectra, p. 20.

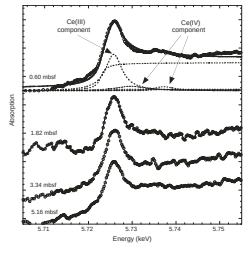

F11. La_N/Ce_N depth profile, p. 21.

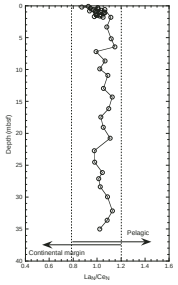

Source Materials of Sediments at Site 1179

The REE signature suggests that the sediment samples from Site 1179 exhibit an intermediate character between pelagic and continental margin sediments. This implication is compared with other geochemical studies. Roser and Korsch (1988) reported a discriminant function dia-

gram for the provenance signatures of sandstone-mudstone suites using major element ratios. Two discriminant functions (DFs) are as below:

$$DF\ 1 = 30.638\ TiO_2/Al_2O_3 - 12.541\ Fe_2O_{3(total)}/Al_2O_3 + 7.329\ MgO/Al_2O_3 + 12.031\ Na_2O/Al_2O_3 + 35.402\ K_2O/Al_2O_3 - 6.382.$$

$$DF\ 2 = 56.500\ TiO_2/Al_2O_3 - 10.879\ Fe_2O_{3(total)}/Al_2O_3 + 30.875\ MgO/Al_2O_3 - 5.404\ Na_2O/Al_2O_3 + 11.112\ K_2O/Al_2O_3 - 3.89.$$

This method was to be used when the influence of biogenic CaO and SiO_2 should be excluded to estimate the provenance of the sediments, which is valid for the samples studied here. Based on the two discriminant functions, as shown in Figure **F12,** our data lie mainly at the boundary of the quartzose sedimentary provenance, the intermediate igneous provenance, and the felsic igneous provenance, suggesting that clastic materials from heterogeneous sources were added to the biogenic silica (diatoms and radiolarians) to produce the sediments at Site 1179. Nakai et al. (1993) studied two sediments in the northwestern Pacific on the basis of REE abundances and Sr and Nd isotopes: one (V20-122) was from 46.3°N, 161.4°E, and the other (RC14-105) was from 39.4°N, 157.3°E. Site 1179 (41.4°N, 159.6°E) is located between these two points. The above study suggested that arc volcanic products and weathered surface matter from the Japanese Islands might be the source of the sediment samples. This is consistent with the interpretation based on the geochemical discrimination diagram, which showed the influence of materials from continents and volcanic products. Further study is required for the distinctive identification of the source material incorporated in the sediments at Site 1179, which show geochemical characteristics pointing to a continental margin, despite the fact that the continents are far away.

F12. Relationship between two discriminant functions, p. 22.

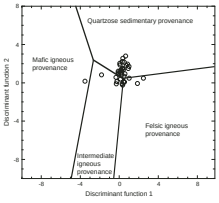

CONCLUSIONS

We tested some geochemical signatures, including the MnO/TiO_2 ratio and La_N/Ce_N ratio, to deduce the depositional environment of the sediments at Site 1179. Among these, diagenetic processes must be taken in to account if the MnO/TiO_2 ratio is to be used to estimate the depositional environment, since the early diagenesis can alter the MnO record in the sediments. Diagenetic transformations of Mn with depth were clearly visible in the profiles of manganese abundances in the sediments and pore waters and with the direct observation of the oxidation state of Mn in the sediments by XANES. REE signatures, such as Ce/Ce* or La_N/Ce_N, can be useful because they are not readily subject to diagenetic effects. However, it is suggested that the Ce/Ce* or La_N/Ce_N ratio should only be used for siliceous sediments. The presence of MnO_2 as a major component in the sediments can cause the lower La_N/Ce_N ratio, which creates a misleading conclusion for the estimation of depositional environment by the La_N/Ce_N ratio. The REE signatures and other geochemical data suggest that a variety of materials from continents and volcanic activities were added to biogenic silica to produce the sediments at Site 1179.

ACKNOWLEDGMENTS

The authors thank M. Nomura, T. Uruga, and K. Okumura for their guidance with the XANES experiments and E. Ohta for carbon analyses. Reviews by Dr. R.W. Murray and an anonymous reviewer have greatly improved this study.

This research used samples provided by the Ocean Drilling Program (ODP). ODP is sponsored by the U.S. National Science Foundation (NSF) and participating countries under management of Joint Oceanographic Institutions (JOI), Inc. Funding for this research was provided by a grant-in-aid for scientific research from the Ministry of Education, Science, Sports and Culture of Japan awarded to Y.T. and H.S. XANES experiments were performed with the approvals of KEK (proposal no. 2000G267) and JASRI (proposal no. 2001B0393-NX-np).

REFERENCES

Anders, E., and Grevesse, N., 1989. Abundances of the elements: meteoritic and solar. *Geochim. Cosmochim. Acta,* 53:197–214.

Froelich, P.N., 1980. Analysis of organic carbon in marine sediments. *Limnol. Oceanogr.,* 25:564–572.

Gromet, L.P., Dymek, R.F., Haskin, L.A., and Korotev, R.L., 1984. The "North American Shale Composite": its compilation, major and trace element characteristics. *Geochim. Cosmochim. Acta,* 48:2469–2482.

Kanazawa, T., Sager, W.W., Escutia, C., et al., 2001. *Proc. ODP, Init. Repts.,* 191 [CD-ROM]. Available from: Ocean Drilling Program, Texas A&M University, College Station TX 77845-9547, USA.

Murray, R.W., 1994. Chemical criteria to identify the depositional environment of chert: general principles and applications. *Sediment. Geol.,* 90:213–232.

Nakai, S., Halliday, A.N., and Rea, D.K., 1993. Provenance of dust in the Pacific Ocean. *Earth Planet. Sci. Lett.,* 119:143–157.

Nomura, M., and Koyama, A., 1996. Design and performance of a new XAFS beamline at the photon factory: BL-12C. *KEK Rep.,* 95-15.

Piepgras, D.J., and Jacobsen, S.B., 1992. The behaviour of rare earth elements in seawater: precise determination of variations in the North Pacific water column. *Geochim. Cosmochim. Acta,* 56:1851–1862.

Roser, B.P., and Korsch, R.J., 1988. Provenance signatures of sandstone-mudstone suites determined using discriminant function analysis of major-element data. *Chem. Geol.,* 67:119–139.

Schulz, H.D., and Zabel, M., 2000. *Marine Geochemistry:* Berlin (Springer).

Schulze, D.G., Sutton, S.R., and Bajt, S., 1995. Determining manganese oxidation state in soils using X-ray-absorption near-edge structure (XANES) spectroscopy. *Soil Sci. Soc. Am. J.,* 59:1540–1548.

Shimizu, H., and Masuda, A., 1977. Cerium in chert as an indication of marine environment of its formation. *Nature,* 266:346–348.

Stein, R., 1986. Organic carbon and sedimentation rate—further evidence for anoxic deep water conditions in the Cenomanian/Turonian Atlantic Ocean. *Mar. Geol.,* 72:199–209.

Stein, R., 1990. Organic carbon/sedimentation rate relationship and its paleoenvironmental significance for marine sediments. *Geo-Mar. Lett.,* 10:37–44.

Sugisaki, R., 1984. Relation between chemical composition and sedimentation rate of Pacific ocean-floor sediments deposited since the middle Cretaceous: basic evidence for chemical constraints on depositional environments of ancient sediments. *J. Geol.,* 92:235–259.

Sugisaki, R., Yamamoto, K., and Adachi, M., 1982. Triassic bedded cherts in central Japan are not pelagic. *Nature,* 298:644–647.

Sugitani, K., 1996. Study of sedimentary paleoenvironments of siliceous sedimentary rocks using some geochemical indicators. *Geochemistry,* 30:75–89. (in Japanese)

Takahashi, Y., Sakami, H., and Nomura, M., 2002a. Determination of the oxidation state of cerium in rocks by Ce L_{III}-edge X-ray absorption near-edge structure spectroscopy. *Anal. Chim. Acta.,* 468:345–54.

Takahashi, Y., Shimizu, H., Kagi, H., Yoshida, H., Usui, A., and Nomura, M. 2000a. A new method for the determination of Ce(III)/Ce(IV) ratios in geological materials: application for weathering, sedimentary, and diagenetic processes. *Earth Planet Sci. Lett.,* 182:201–207.

Takahashi, Y., Shimizu, H., Usui, A., Kagi, H., and Nomura, M. 2000b. Direct observation of tetravalent cerium in ferromanganese nodules and crusts by X-ray-absorption near-edge structure (XANES). *Geochim. Cosmochim. Acta,* 64:2929–2935.

Takahashi, Y., Yoshida, H., Sato, N., Hama, K., Yusa, Y., and Shimizu, H. 2002b. W- and M-type tetrad effects in REE patterns for water-rock systems in the Tono uranium deposit, central Japan. *Chem. Geol.,* 184:311–335.

Taylor, S.R., and McLennan, S.M., 1988. The significance of the rare earths in geochemistry and cosmochemistry. *In* Gschneidner, K.A., Jr., and Eyring, L. (Eds.), *Handbook on the Physics and Chemistry of Rare Earth* (Vol. 11): Amsterdam (Elsevier), 485–578.

Uruga, T., Tanida, H., Yoneda, Y., Takeshita, K., Emura, S., Takahashi, M., Harada, M., Nishihata, Y., Kubozono, Y., Tanaka, T., Yamamoto, T., Maeda, H., Kamishima, O., Takabayashi, Y., Nakata, Y., Kimura, H., Goto, S., and Ishikawa, T., 1999. The XAFS beamline BL01B1 at SPring-8. *J. Synchrotron Radiat.,* 6:143–145.

Yamamoto, K., 1983. Geochemical study of Triassic bedded cherts from Kamiaso, Gifu Prefecture. *Chishitsugaku Zasshi,* 89:143–162. (in Japanese)

Figure F1. Map of Site 1179, studied in this paper.

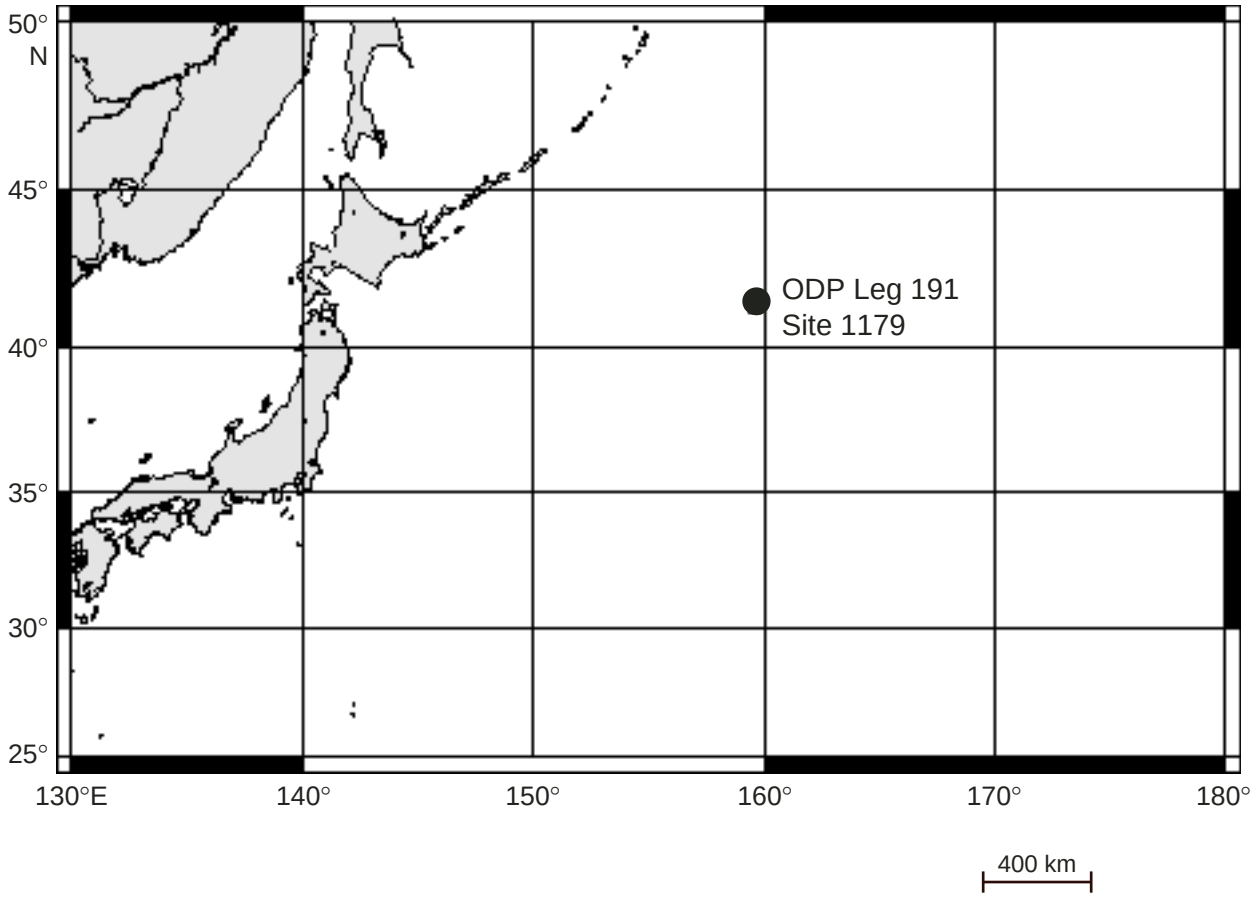

Figure F2. Depth profile of dissolved Mn and SO_4 in pore water of sediments at Site 1179 (Kanazawa, Sager, Escutia, et al., 2001).

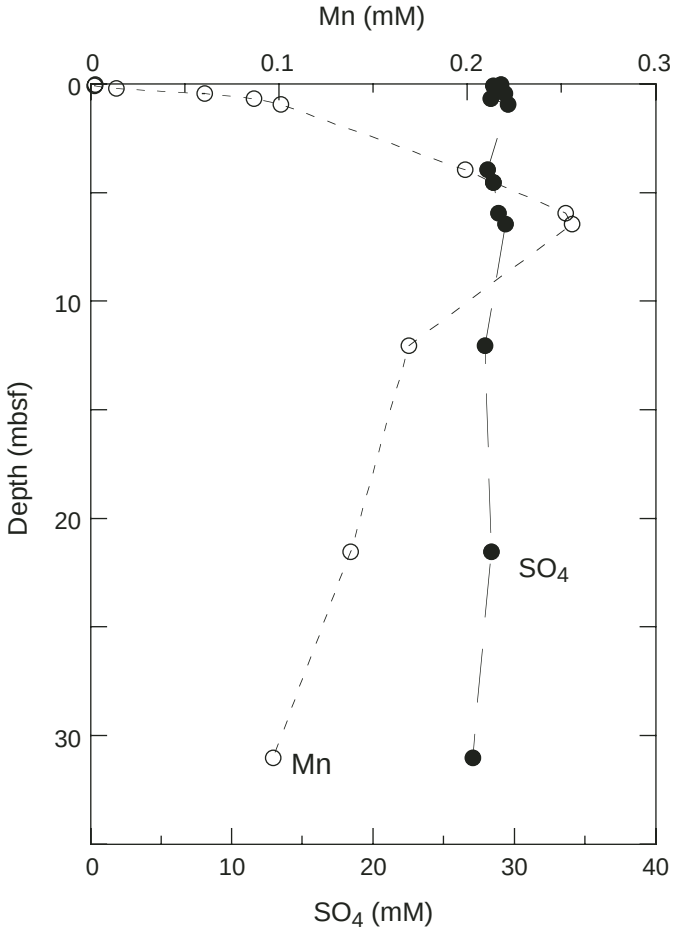

Figure F3. A. Spectra of Mn K-edge XANES for the reference materials made by mixing $Mn(II)SO_4$ and δ-$Mn(IV)O_2$. Total concentration of Mn was 2000 ppm adjusted by diluting with quartz sand. The molar ratio of Mn(II) and Mn(IV) is indicated in the figure. **B.** The relationship between the average valence of Mn and the energy shift of the pre-edge peak in the reference material from the pre-edge of δ-MnO_2. **C.** An example of fitting results of the pre-edge of Mn K-edge XANES for sediment samples from 0.60 and 1.82 mbsf recovered from Hole 1179B cores. It is clearly observed that Mn at 1.82 mbsf is more reduced than that at 0.60 mbsf.

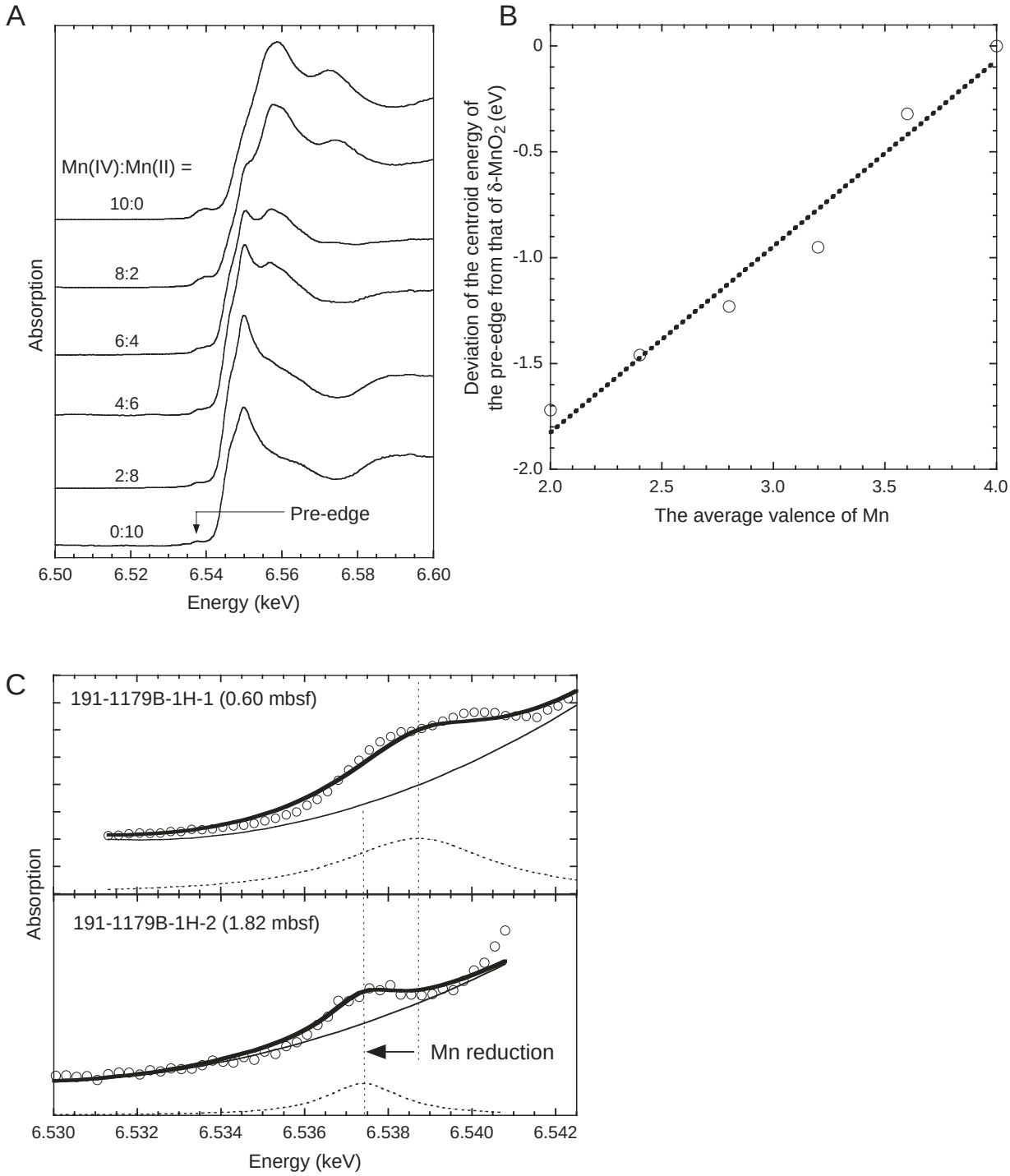

Figure F4. Depth profile of the average valence of Mn determined by XANES.

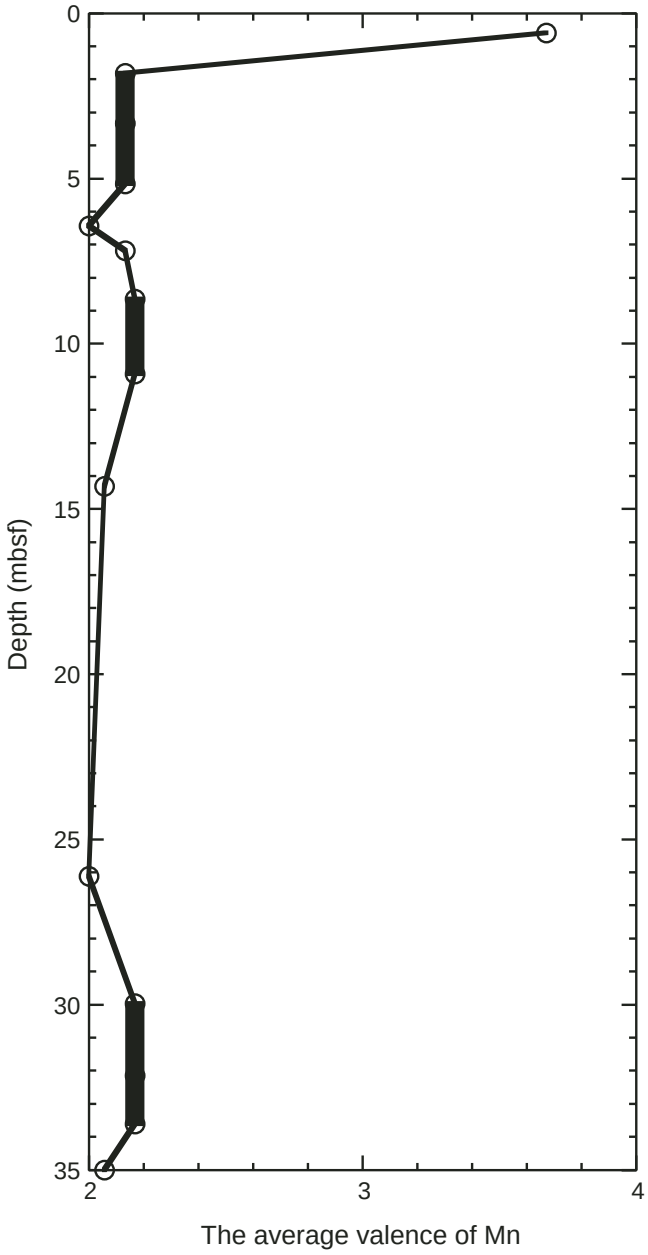

Figure F5. Relationship between the MnO/TiO_2 ratio in marine sediments and the distance from land. Original data were listed in Sugitani (1996).

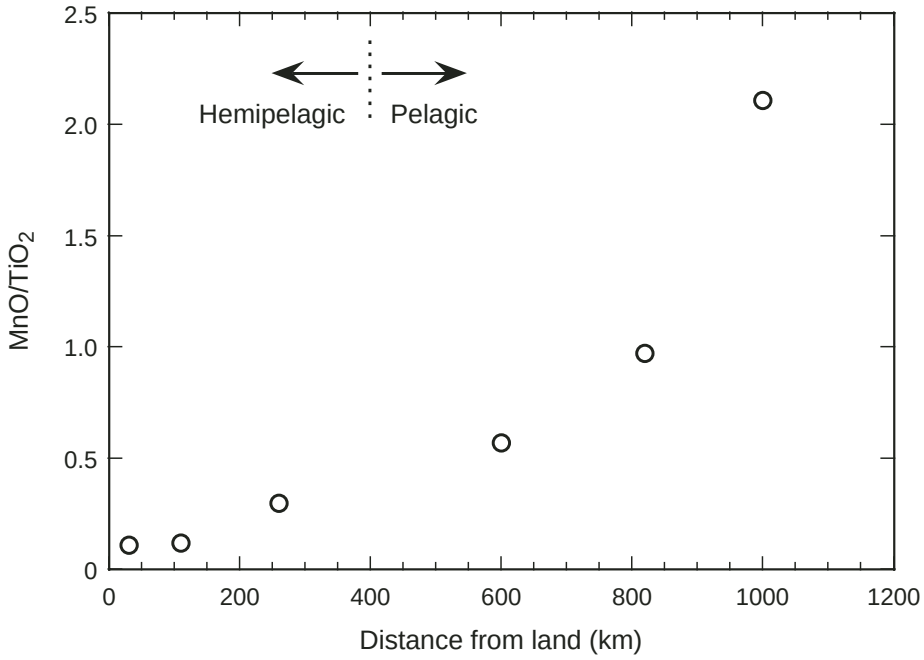

Figure F6. Depth profile of the MnO/TiO_2 ratio of sediments recovered from Site 1179.

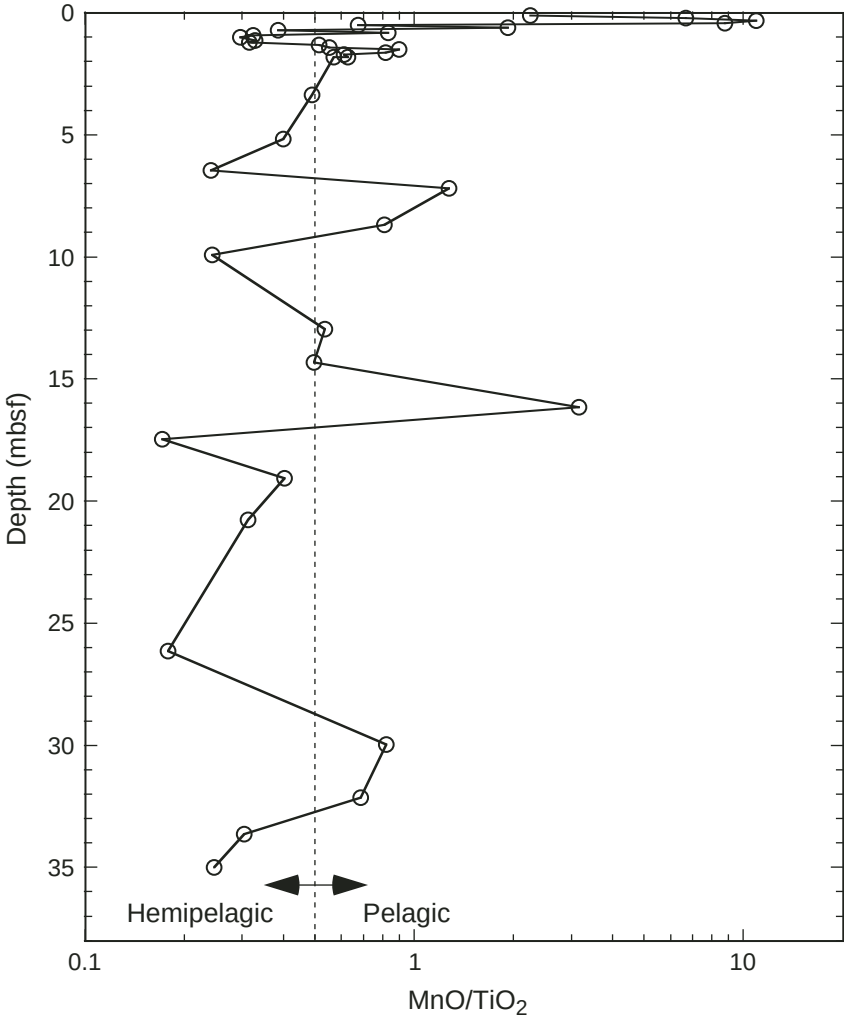

Figure F7. Post-Archean shales from Australia (PAAS)-normalized REE patterns of sediment recovered from (**A**) Core 191-1179C-1H and (**C**) Cores 191-1179B-1H through 4H, and (**B**) samples employed for the Ce L_{III}-edge analysis at Site 1179 (Core 191-1179B-1H).

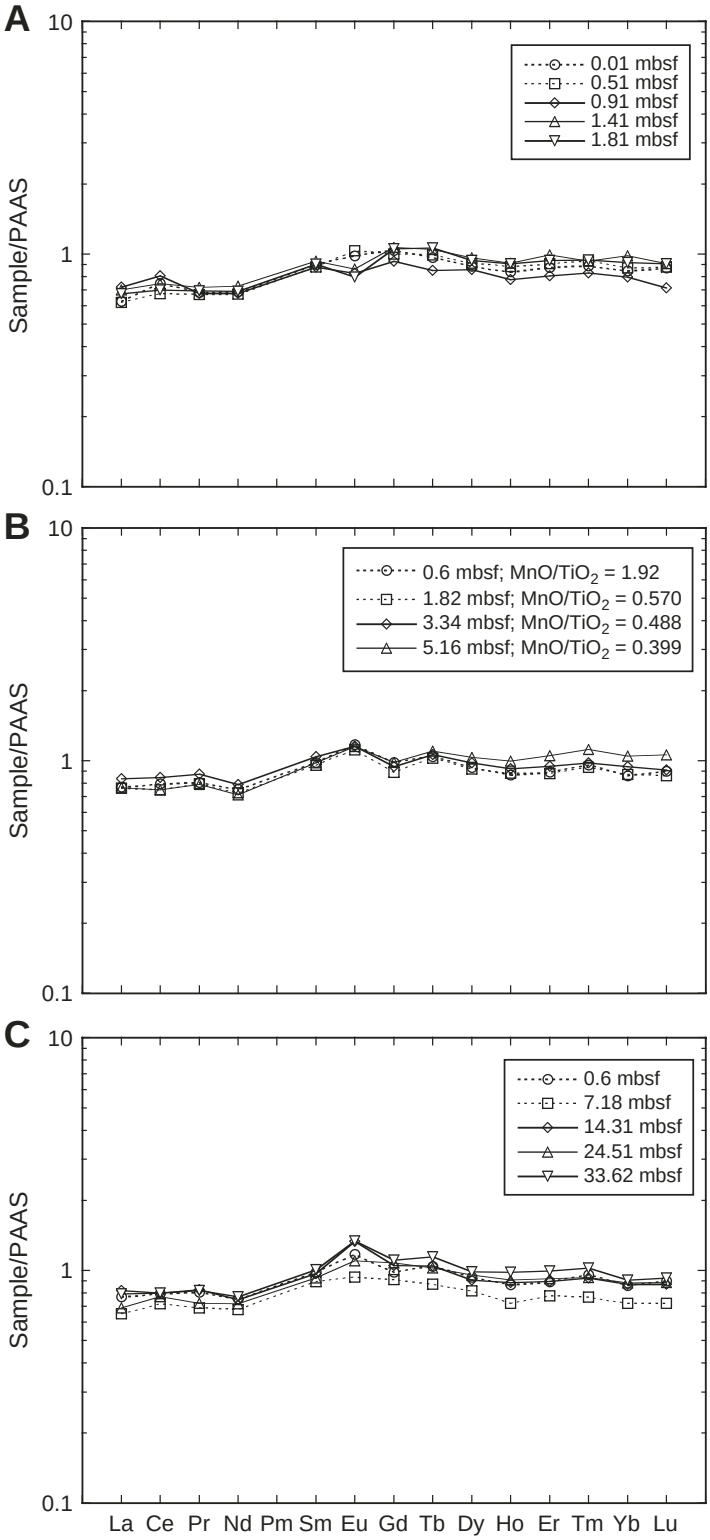

Figure F8. Relationship between Nd and TiO_2 for the sediment samples recovered from Hole 1179B.

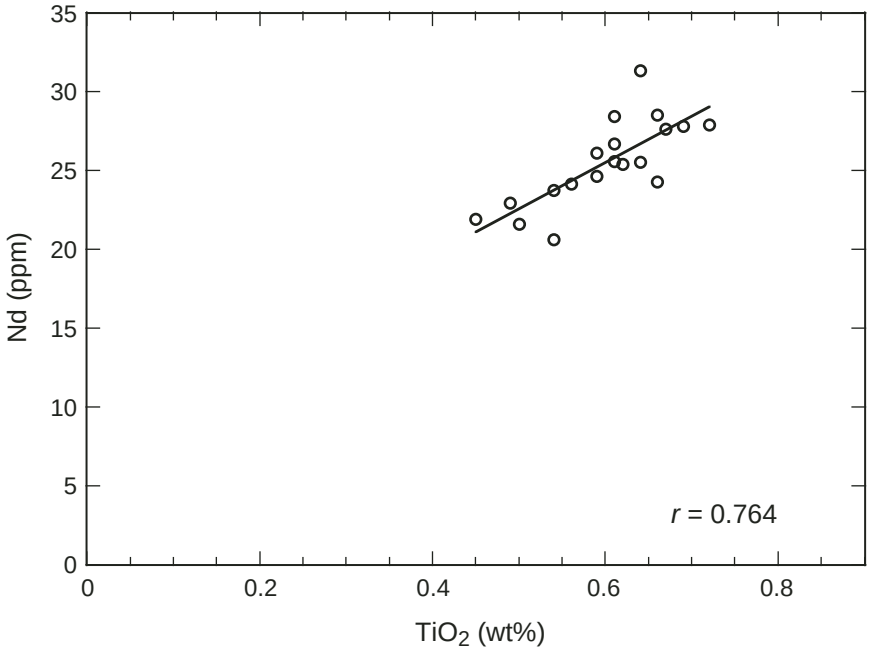

Figure F9. Relationship between the La_N/Ce_N ratio and $Al_2O_3/(Al_2O_3+Fe_2O_3)$ for the sediment samples from Site 1179. The field of each depositional environment was reported in Murray (1994).

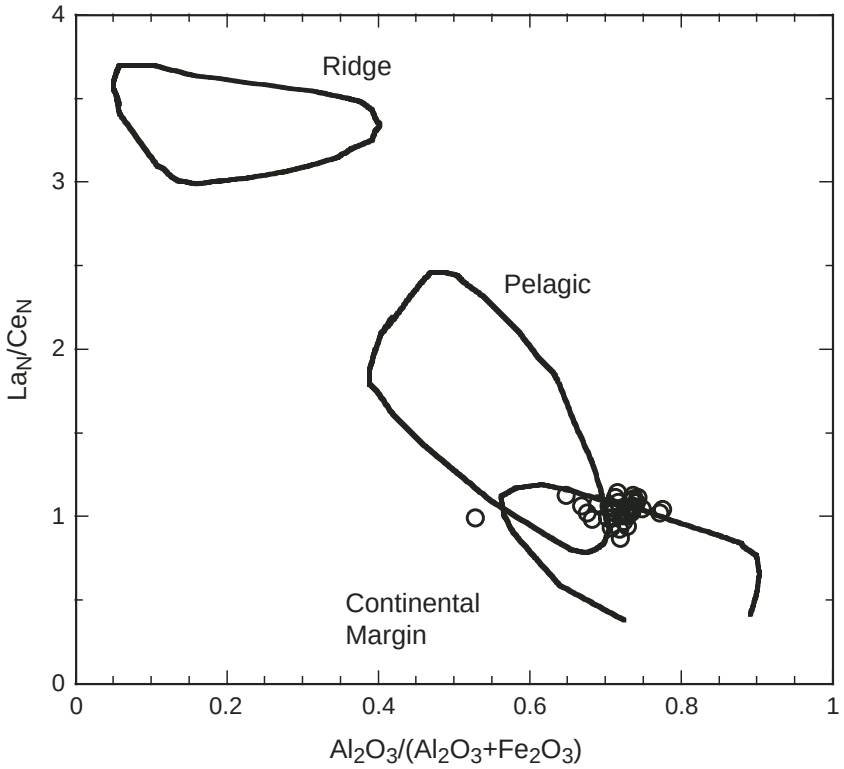

Figure F10. Cerium L_{III}-edge XANES spectra of some sediment samples from Site 1179.

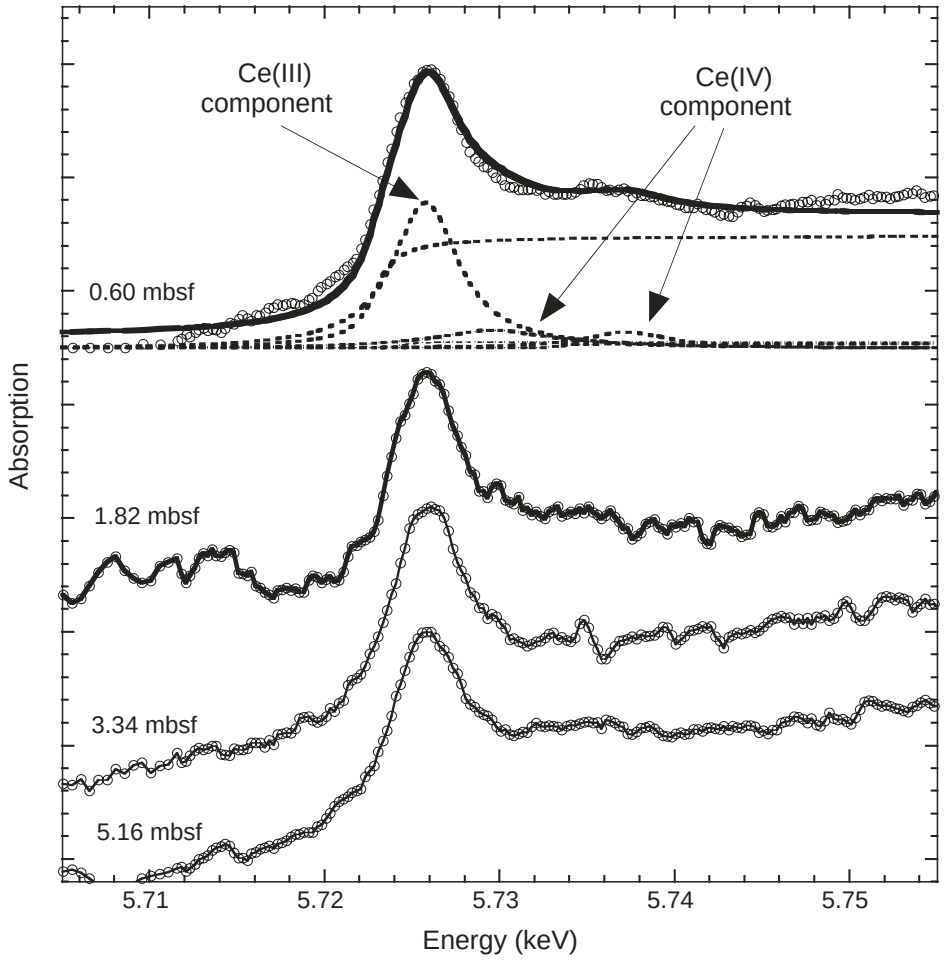

Figure F11. Depth profile of the La_N/Ce_N ratio of sediments recovered from Site 1179.

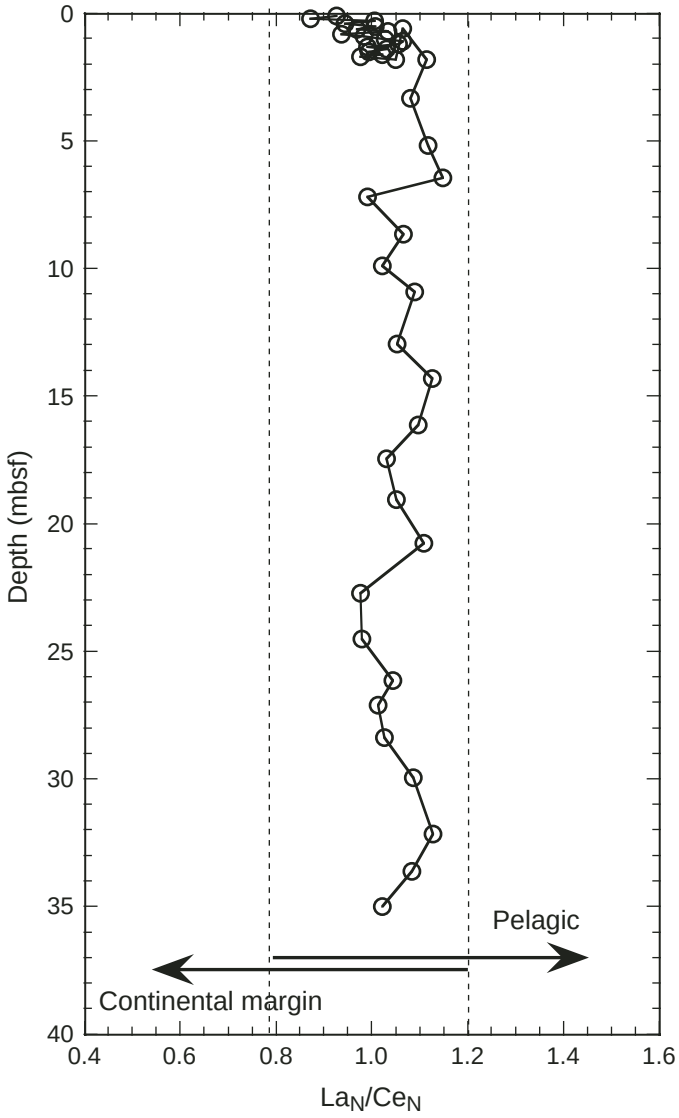

Figure F12. Relationship between two discriminant functions (DFs) (Roser and Korsch, 1988) for the sediment samples from Site 1179. DF 1 = 30.638 TiO_2/Al_2O_3 – 12.541 $Fe_2O_{3(total)}/Al_2O_3$ + 7.329 MgO/Al_2O_3 + 12.031 Na_2O/Al_2O_3 + 35.402 K_2O/Al_2O_3 – 6.382. DF 2 = 56.500 TiO_2/Al_2O_3 – 10.879 $Fe_2O_{3(total)}/Al_2O_3$ + 30.875 MgO/Al_2O_3 – 5.404 Na_2O/Al_2O_3 + 11.112 K_2O/Al_2O_3 – 3.89. (For more information on DFs, see **"Source Materials of Sediments at Site 1179,"** p. 6, in "Results and Discussion").

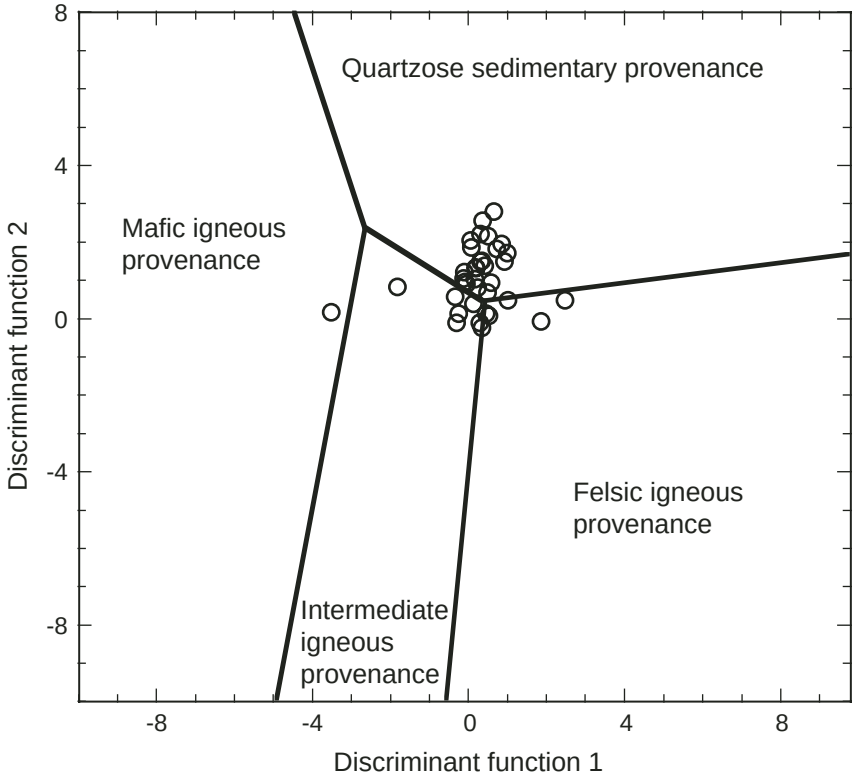

Table T1. Major element composition of sediment samples recovered from Cores 191-1179C-1H and 191-1179B-1H through 4H.

Core, section, interval (cm)	Depth (mbsf)	Major element oxide (wt%)										LOI (wt%)	C (wt%)		Description
		SiO_2	TiO_2	Al_2O_3	Fe_2O_3*	MnO	MgO	CaO	Na_2O	K_2O	P_2O_5		(organic)	(inorganic)	
191-1179B-															
1H-1	0.60	58.20	0.61	13.83	5.81	1.16	2.69	1.42	2.74	2.50	0.11	10.65	0.40	0.31	Siliceous ooze
1H-2	1.82	60.39	0.59	13.88	5.58	0.34	2.75	1.42	2.57	2.60	0.09	9.55	0.41	0.26	Siliceous ooze
1H-3	3.34	58.31	0.61	14.04	6.32	0.30	2.98	1.09	2.75	2.77	0.09	10.51	0.40	0.18	Siliceous ooze and clay
1H-4	5.16	60.09	0.56	13.72	4.77	0.22	2.32	1.40	3.40	2.43	0.08	10.61	0.36	0.21	Siliceous ooze
1H-5	6.45	59.41	0.54	13.79	5.48	0.13	2.49	1.16	3.55	2.41	0.08	10.67	0.26	0.08	Siliceous ooze
1H-5	7.18	57.17	0.49	11.37	10.17	0.63	3.73	0.99	2.51	2.47	0.07	10.17	0.37	0.42	Siliceous ooze
2H-1	8.66	58.17	0.61	14.02	6.95	0.50	3.27	1.00	3.01	2.89	0.08	9.20	0.44	0.19	Siliceous ooze and clay
2H-2	9.89	66.01	0.50	13.79	4.08	0.12	1.85	1.38	3.37	2.69	0.07	5.88	0.20	0.06	Siliceous ooze
2H-3	10.92	—	—	—	—	—	—	—	—	—	—	—	0.50	0.27	Siliceous ooze and clay
2H-4	12.94	59.91	0.64	15.04	6.19	0.34	3.04	1.10	2.64	2.95	0.09	7.84	0.42	0.29	Siliceous ooze and clay
2H-5	14.31	58.03	0.62	14.61	7.95	0.31	3.20	0.97	1.86	2.86	0.08	9.04	0.19	0.11	Siliceous ooze
2H-6	16.14	56.73	0.67	15.36	5.56	2.12	3.00	1.41	1.86	3.03	0.11	9.90	0.32	0.62	Siliceous ooze and clay
3H-1	17.47	62.65	0.64	15.32	5.70	0.11	2.59	1.15	2.29	2.89	0.08	6.31	0.20	0.17	Siliceous ooze and clay
3H-2	19.05	60.26	0.72	16.29	5.49	0.29	3.30	1.13	1.82	3.25	0.09	7.12	0.43	0.28	Siliceous ooze
3H-3	20.76	58.88	0.69	15.74	5.60	0.22	2.99	1.08	1.87	2.99	0.08	9.60	0.40	0.21	Siliceous ooze
3H-4	22.71	—	—	—	—	—	—	—	—	—	—	—	0.12	0.13	Siliceous ooze and clay
3H-5	24.51	62.74	0.55	13.95	6.08	0.18	2.60	1.08	2.17	2.64	0.07	7.52	0.19	0.19	Siliceous ooze and clay
3H-6	26.13	63.91	0.45	13.95	4.06	0.08	1.85	1.07	2.54	3.29	0.07	8.51	0.14	0.05	Siliceous ooze and clay
4H-1	27.10	—	—	—	—	—	—	—	—	—	—	—	0.42	0.18	Siliceous ooze
4H-2	28.38	—	—	—	—	—	—	—	—	—	—	—	0.33	0.34	Siliceous ooze
4H-3	29.96	58.57	0.66	15.61	5.47	0.54	2.89	1.14	1.85	2.99	0.08	9.97	0.35	0.28	Siliceous ooze and clay
4H-4	32.14	58.38	0.66	15.38	5.51	0.45	3.16	1.46	1.76	3.05	0.09	9.86	0.43	0.32	Clay
4H-5	33.62	59.53	0.59	14.15	5.60	0.18	2.53	1.05	2.03	2.76	0.07	11.26	0.29	0.10	Siliceous ooze and clay
4H-6	35.00	60.07	0.54	13.69	5.18	0.13	2.40	0.98	2.38	2.62	0.06	11.68	0.40	0.07	Ash
191-1179C-															
1H-1, 0–2	0.01	—	—	—	—	—	—	—	—	—	—	—	0.52	0.23	Siliceous ooze
1H-1, 10–12	0.11	52.95	0.52	13.95	5.46	1.18	2.40	1.25	3.13	2.31	0.13	16.31	0.41	0.27	Siliceous ooze and clay
1H-1, 20–22	0.21	57.49	0.52	13.51	5.26	3.44	2.32	1.34	3.61	2.27	0.13	9.72	0.18	0.20	Siliceous ooze and clay
1H-1, 30–32	0.31	57.55	0.51	13.22	4.94	5.52	2.20	1.52	3.26	2.23	0.12	8.57	0.23	0.21	Siliceous ooze and clay
1H-1, 40–42	0.41	57.21	0.53	13.19	4.91	4.68	2.28	1.63	3.51	2.18	0.13	9.44	0.31	0.20	Siliceous ooze and clay
1H-1, 50–52	0.51	61.35	0.61	14.55	5.61	0.41	2.48	1.74	3.21	2.38	0.12	7.31	0.47	0.13	Siliceous ooze
1H-1, 60–62	0.61	—	—	—	—	—	—	—	—	—	—	—	0.40	0.25	Siliceous ooze and clay
1H-1, 70–72	0.71	60.79	0.62	14.25	5.91	0.24	2.79	1.27	2.89	2.63	0.10	8.26	0.54	0.14	Siliceous ooze and clay
1H-1, 80–82	0.81	60.09	0.60	13.84	5.72	0.50	2.84	1.11	2.82	2.61	0.10	9.52	0.43	0.24	Siliceous ooze and clay
1H-1, 90–92	0.91	60.23	0.63	14.10	6.55	0.20	3.02	1.15	2.78	2.70	0.10	8.32	0.51	0.21	Siliceous ooze and clay
1H-1,100–102	1.01	62.55	0.65	14.82	5.36	0.19	2.98	1.20	2.25	2.84	0.09	6.83	0.47	0.24	Siliceous ooze and clay
1H-1, 110–112	1.11	60.68	0.62	14.13	5.10	0.20	2.78	1.31	2.59	2.65	0.09	9.60	0.43	0.23	Siliceous ooze and clay
1H-1, 120–122	1.21	61.02	0.63	14.60	5.23	0.20	2.94	1.30	2.71	2.75	0.09	8.27	0.42	0.20	Siliceous ooze and clay
1H-1, 130–132	1.31	61.96	0.59	13.85	5.85	0.30	2.67	1.76	3.02	2.34	0.10	7.33	0.30	0.16	Siliceous ooze and clay
1H-1, 140–142	1.41	61.23	0.56	13.67	5.58	0.31	2.70	1.36	3.12	2.55	0.09	8.59	0.38	0.15	Siliceous ooze and clay
1H-2, 150–152	1.51	62.54	0.55	13.44	5.50	0.49	2.53	1.38	2.93	2.56	0.09	10.67	0.30	0.19	Siliceous ooze and clay
1H-2, 160–162	1.61	61.74	0.52	12.96	6.21	0.42	2.65	1.36	3.03	2.56	0.09	8.23	0.31	0.24	Siliceous ooze and clay
1H-2, 170–172	1.71	61.76	0.58	13.74	5.24	0.35	2.75	1.37	2.89	2.64	0.09	8.32	0.43	0.26	Siliceous ooze and clay
1H-2, 180–182	1.81	62.92	0.56	13.21	4.90	0.35	2.67	1.38	2.68	2.54	0.09	8.40	0.52	0.31	Siliceous ooze and clay

Notes: * = total Fe as Fe_2O_3. LOI = loss on ignition at 110°C, — = baking.

Table T2. Abundances of REE in sediment samples recovered from Cores 191-1179C-1H and 191-1179B-1H through 4H.

Core, section, interval (cm)	Depth (mbsf)	Rare earth element (ppm)													
		La	Ce	Pr	Nd	Sm	Eu	Gd	Tb	Dy	Ho	Er	Tm	Yb	Lu
191-1179B-															
1H-1	0.60	29.5	63.3	7.12	25.6	5.45	1.27	4.58	0.806	4.38	0.861	2.55	0.388	2.43	0.391
1H-2	1.82	29.0	59.5	7.04	24.7	5.29	1.20	4.15	0.794	4.30	0.874	2.50	0.379	2.46	0.373
1H-3	3.34	32.0	67.5	7.75	26.7	5.78	1.25	4.39	0.825	4.59	0.917	2.70	0.396	2.66	0.396
1H-4	5.16	29.2	59.7	6.97	24.2	5.43	1.25	4.58	0.850	4.83	0.989	3.00	0.452	2.95	0.458
1H-5	6.45	26.1	51.9	6.03	20.6	4.46	1.04	3.41	0.654	3.70	0.759	2.31	0.340	2.28	0.358
1H-5	7.18	24.9	57.3	6.09	23.0	4.97	1.01	4.26	0.675	3.82	0.716	2.22	0.310	2.04	0.312
2H-1	8.66	33.6	72.0	8.14	28.5	5.90	1.29	4.47	0.845	4.53	0.901	2.69	0.381	2.51	0.374
2H-2	9.89	21.9	48.9	5.58	21.6	4.76	1.03	4.65	0.794	4.66	0.957	3.08	0.447	2.96	0.462
2H-3	10.92	34.5	72.3	8.31	28.6	6.07	1.31	4.61	0.856	4.59	0.913	2.68	0.396	2.56	0.395
2H-4	12.94	34.6	75.0	8.34	31.4	6.66	1.39	5.88	0.933	5.45	1.044	3.18	0.431	2.90	0.441
2H-5	14.31	31.4	63.6	7.30	25.4	5.39	1.44	4.90	0.808	4.26	0.881	2.56	0.375	2.45	0.377
2H-6	16.14	32.7	68.1	7.86	27.7	5.98	1.49	5.47	0.944	5.19	1.078	3.26	0.480	3.17	0.506
3H-1	17.47	28.4	62.8	6.81	25.6	5.53	1.17	5.14	0.800	4.55	0.923	2.79	0.395	2.65	0.404
3H-2	19.05	31.8	69.0	7.52	27.9	5.74	1.25	5.21	0.826	4.70	0.951	2.80	0.414	2.70	0.402
3H-3	20.76	32.6	67.1	7.94	27.9	5.88	1.37	5.15	0.887	4.64	0.948	2.74	0.399	2.59	0.402
3H-4	22.71	17.5	41.0	4.58	18.1	4.22	0.98	4.13	0.675	4.06	0.811	2.43	0.349	2.32	0.364
3H-5	24.51	26.4	61.4	6.38	24.3	5.15	1.19	5.02	0.792	4.47	0.899	2.63	0.378	2.49	0.384
3H-6	26.13	26.2	57.2	6.30	21.9	4.65	1.16	4.33	0.738	4.12	0.849	2.59	0.381	2.59	0.401
4H-1	27.10	31.9	71.9	7.50	28.9	6.00	0.99	5.30	0.921	4.99	1.053	3.05	0.444	3.10	0.434
4H-2	28.38	30.3	67.4	7.12	27.2	5.64	1.04	5.49	0.925	5.03	1.047	3.41	0.500	3.43	0.492
4H-3	29.96	29.3	61.6	6.97	24.3	5.08	1.25	4.71	0.823	4.38	0.926	2.74	0.405	2.70	0.434
4H-4	32.14	33.8	68.3	8.17	28.5	6.13	1.45	5.61	0.898	4.72	0.974	2.83	0.407	2.66	0.399
4H-5	33.62	30.3	63.8	7.26	26.1	5.58	1.45	5.15	0.886	4.62	0.977	2.84	0.415	2.56	0.402
4H-6	35.00	27.7	61.9	6.62	23.8	5.22	1.27	4.84	0.825	4.44	0.901	2.62	0.378	2.53	0.393
191-1179C-															
1H-1, 0–2	0.01	24.0	59.7	6.05	23.4	5.00	1.06	4.83	0.750	4.16	0.830	2.50	0.361	2.39	0.377
1H-1, 10–12	0.11	23.0	56.7	5.77	22.4	4.85	1.06	4.59	0.740	4.10	0.824	2.46	0.360	2.34	0.372
1H-1, 20–22	0.21	27.3	71.6	6.31	24.8	5.47	1.08	5.26	0.818	4.83	0.899	2.84	0.411	2.82	0.411
1H-1, 30–32	0.31	21.2	48.0	5.30	20.9	4.53	1.02	4.33	0.712	3.99	0.826	2.45	0.359	2.39	0.382
1H-1, 40–42	0.41	21.8	52.7	5.50	21.6	4.65	1.07	4.69	0.755	4.21	0.876	2.59	0.374	2.43	0.379
1H-1, 50–52	0.51	23.7	53.8	5.93	22.8	4.88	1.12	4.67	0.764	4.28	0.874	2.59	0.378	2.45	0.381
1H-1, 60–62	0.61	25.7	60.5	6.39	24.6	5.20	1.15	4.89	0.778	4.28	0.865	2.58	0.365	2.42	0.364
1H-1, 70–72	0.71	24.9	54.9	6.07	23.1	4.80	1.01	4.36	0.708	3.90	0.779	2.29	0.329	2.19	0.331
1H-1, 80–82	0.81	28.3	69.0	6.24	23.9	5.14	0.96	4.56	0.712	4.20	0.787	2.46	0.343	2.32	0.331
1H-1, 90–92	0.91	27.6	64.0	5.98	23.0	4.88	0.89	4.33	0.658	4.02	0.770	2.30	0.336	2.24	0.310
1H-1, 100–102	1.01	29.1	64.6	6.87	27.2	5.98	1.20	5.52	0.827	4.86	0.908	2.81	0.413	2.84	0.411
1H-1, 110–112	1.11	26.6	57.1	6.16	24.7	5.34	1.12	5.13	0.771	4.49	0.861	2.63	0.383	2.55	0.367
1H-1, 120–122	1.21	26.2	56.6	6.08	24.7	5.54	1.10	5.16	0.811	4.78	0.893	2.78	0.404	2.61	0.380
1H-1, 130–132	1.31	23.9	55.0	5.72	23.3	5.48	1.19	5.48	0.818	4.82	0.933	2.76	0.404	2.72	0.403
1H-1, 140–142	1.41	26.8	59.3	6.33	24.7	5.16	0.93	4.97	0.810	4.50	0.904	2.83	0.378	2.77	0.393
1H-1, 150–152	1.51	20.5	47.2	5.04	19.9	4.20	0.71	3.96	0.653	3.68	0.758	2.27	0.320	2.23	0.344
1H-1, 160–162	1.61	26.1	58.3	6.33	25.4	5.58	1.09	5.13	0.859	4.80	1.030	2.97	0.425	2.88	0.434
1H-1, 170–172	1.71	30.1	70.3	7.49	29.2	6.44	1.14	5.64	0.963	5.01	0.997	2.99	0.434	2.84	0.409
1H-1, 180–182	1.81	25.7	55.9	6.15	23.4	5.02	0.86	4.91	0.822	4.40	0.898	2.68	0.382	2.60	0.393